

Dispersion of the Nonlinear Optical Susceptibility $\chi^{(3)}$ in n -InSb in a Magnetic Field

J. J. Wynne

IBM Thomas J. Watson Research Center, Yorktown Heights, New York 10598

(Received 21 December 1971)

A simple semiclassical model for the nonparabolic conduction band of InSb is used to calculate the third-order nonlinear optical susceptibility $\chi^{(3)}(-\omega_3, \omega_1, \omega_1, -\omega_2)$ in the presence of a dc magnetic field. In particular, we find resonant contributions when the difference frequency $\omega_2 - \omega_1$ is near the cyclotron frequency or twice the cyclotron frequency. The results of this model are compared to earlier experimental results.

I. INTRODUCTION

The study of the dispersive behavior of nonlinear optical susceptibilities has long been recognized as a potentially fruitful method of learning new information about the electronic structure of solids. Nevertheless, relatively few useful studies of the nonlinear dispersion have been carried out, although the picture is expected to change in the near future with the current and growing availability of tunable coherent sources of light such as dye lasers. Soref and Moos¹ were the first to report on the dispersive behavior of the susceptibility $\chi^{(2)}(-2\omega, \omega, \omega)$ describing second harmonic generation (SHG). They measured SHG as a function of alloy composition in wurtzite ZnS-CdS and CdS-CdSe single crystals, using a fixed frequency laser as the source of the fundamental wave. $\chi^{(2)}$ was observed to vary monotonically with band gap. A theory based upon a spherical band model, with gaps and curvatures taken from the literature, gave a good fit to the experiment. To quote Soref and Moos, "If the properties of the semiconductor alloy series are such that varying the band gap by alloying is equivalent to shifting the applied laser frequency, the dispersion of the second-order susceptibility has been determined." The need to make such a shaky assumption has, unfortunately, limited the usefulness of studies of this type.

Chang, Ducuing, and Bloembergen² reported on the direct measurement of the dispersion of $\chi^{(2)}$ in several semiconductors having the zinc-blende structure. They used several discrete-frequency sources to provide radiation at the fundamental frequency and observed large variations in $\chi^{(2)}$. They linked these variations with the resonant behavior of electronic states at the critical points in the joint density of states of the valence and conduction bands. More recently, Parsons and Chang³ reported on the dispersion of $\chi^{(2)}$ in three of the materials studied earlier by Chang *et al.*² Parsons and Chang used continuously tunable dye lasers and their results differ somewhat from the earlier results. I have recently reported on the dispersion of $\chi^{(2)}$ in InSb.⁴ I used the different discrete lines

of a CO₂ laser and tuned through a small frequency range, varying the second-harmonic photon energy over a small range near the minimum-band-gap energy. My results show surprisingly large changes of $\chi^{(2)}$ over this small frequency range. A correct interpretation of this result may provide heretofore unavailable information about the effect of the asymmetric crystalline potential on electronic states (and consequently the momentum matrix elements) near $\vec{k}=0$ in the Brillouin zone.

We expect to see interesting dispersive behavior when the excitation frequencies (or combinations of frequencies) become coincident with some material-system resonance. This approach was employed in Refs. 2-4. However, rather than varying the excitation frequencies, one may keep them fixed and tune the material resonance by changing some other property. This latter method characterizes the approach I have taken in the work to be reported in this paper. Soref and Moos's¹ work also belongs to this category, but the interpretation of their results is not as transparent because the parameter which they varied (composition) has a multifold effect upon all the material properties.

We have studied the nonlinear susceptibility $\chi^{(3)}(-\omega_3, \omega_1, \omega_1, -\omega_2)$, which describes optical-frequency mixing of the form $\omega_3 = 2\omega_1 - \omega_2$. In an earlier publication, Yablonovitch, Bloembergen, and Wynne⁵ (hereafter referred to as YBW) reported the experimental results of the study of $\chi^{(3)}$ in n -InSb as a function of magnetic field. YBW used the experimental geometry shown in Fig. 1 to detect light at ω_3 , where ω_1 and ω_2 were the frequencies of radiation emitted by a Q-switched CO₂ laser. Their experimental results are presented in Fig. 2. The reader is referred to YBW for further experimental details. Basically, the material resonance which contributes to the dispersion of $\chi^{(3)}$ involves single-electron transitions between Landau levels within the conduction band. The frequencies ω_1 , ω_2 , and ω_3 were all much larger than the cyclotron frequency ω_c , even for the largest magnetic field (23 kG) used. YBW observed resonant enhancement when the difference frequency $\Delta\omega = |\omega_2 - \omega_1|$ was near ω_c or $2\omega_c$. They point out

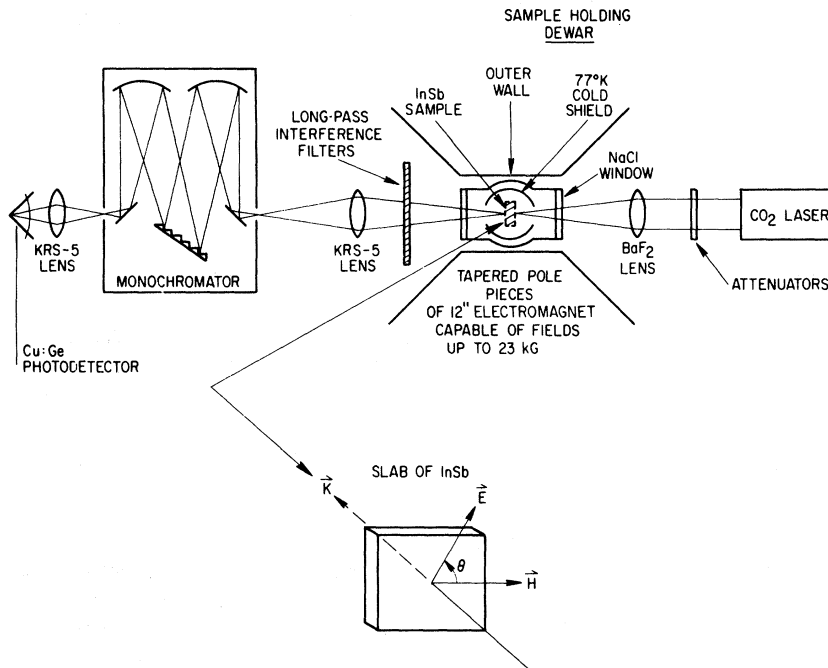


FIG. 1. Experimental sample and detection geometry.

the connection between this effect and Raman scattering. In fact, it was the observation of Raman scattering from Landau levels in n -InSb, as reported by Patel and co-workers,⁶ which provided the impetus to YBW. They recognized that the same physical phenomena which give rise to Raman scattering, also contribute a resonant term to the real part of the Raman-type susceptibility $\chi^{(3)}$ ($-\omega_3, \omega_1, \omega_2, -\omega_1$). In order to observe the Raman scattering, the scattered light must be detected against a background of elastically scattered light. A narrow linewidth and a large cross section are two assets which enhance the detectability of Raman-scattered light. Analogously, the resonant contribution to $\chi^{(3)}$ is more easily observable if the resonance is sharp and the resonant term is sizeable relative to the nonresonant "background." The "background" is due to other material transitions far from resonance. In particular, in InSb there is a large nonresonant contribution due to the nonparabolic conduction-band electrons in the absence of a dc magnetic field. YBW briefly mentioned a simple semiclassical treatment of the nonparabolic conduction band of InSb including magnetic field, which gives qualitative agreement with experiment. A more detailed discussion of this treatment and a careful comparison with experiment are the main themes of this paper.

In Sec. II the model is discussed. A physical picture of the resonant enhancement and relevant selection rules is given. Section III is a comparison of theory and experiment, and Sec. IV is a discussion of some of the limitations of this model.

II. THEORY

There are several aspects of the experimental results which a reasonable model ought to be able to explain. They are (i) the strength of the resonant enhancement, (ii) the position of the S-like dispersion curves as a function of the dc magnetic field, (iii) the dependence on the angle θ between the magnetic field and the electric fields of the light waves, and (iv) the asymptotic limit for large magnetic fields. All of these are to some degree accounted for by our model. The model is based on a simple semiclassical treatment of the nonparabolic conduction band in InSb. Wolff and Pearson⁷ first used it to account for the large three-wave mixing observed in InSb and InAs⁸ in the absence of a dc magnetic field. Lax, Zawadski, and Weiler⁹ extended it to include the magnetic field, and we extend it even further to include terms ignored by Lax *et al.*⁹ These terms are higher order in the crystal momentum than those considered by Lax *et al.*, but they become resonant at much lower magnetic fields. The remainder of this section is concerned with the details of this model. The reader who is mainly interested in the comparison with experimental results may skip to Sec. III. In Sec. III reference will be made to the results from Sec. II which are necessary for the comparison.

The crucial point in considering frequency mixing due to nonparabolicity is that the electron's velocity is a nonlinear function of its momentum. Also, in the presence of a dc magnetic field, the Lorentz force provides an additional source of nonlinearity

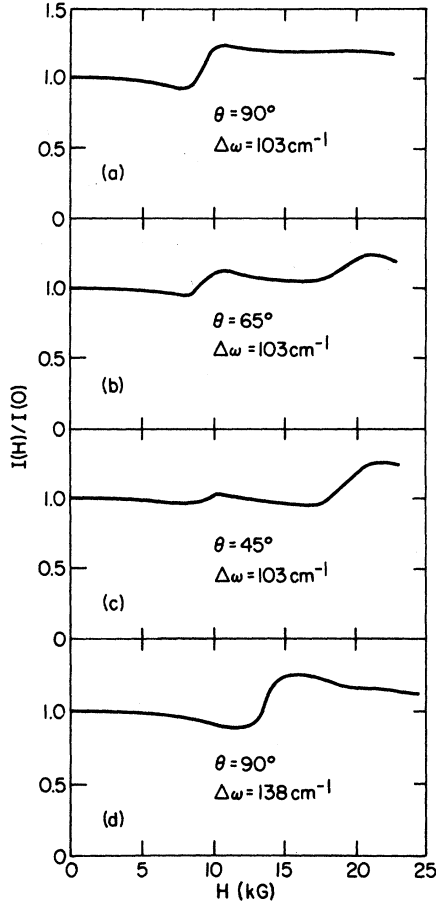


FIG. 2. Output power at ω_3 as a function of magnetic field. \vec{E} is the electric field vector and \vec{H} the magnetic field vector. In (a), (b), and (c) ω_1 is 944 cm^{-1} and ω_2 is 1047 cm^{-1} , whereas in (d) ω_2 is 1082 cm^{-1} . The curves are normalized at $H=0$ and the accuracy in the experimental power data at the high-field end is about 4% (Ref. 5).

proportional to the magnetic field.

We proceed by describing the unperturbed motion of a single electron in the conduction band by Kane's¹⁰ Hamiltonian

$$\epsilon = \frac{1}{2}\epsilon_G[(1 + 2p^2/m^*\epsilon_G)^{1/2} - 1], \quad (1)$$

where ϵ_G is the band gap, m^* is the band-edge effective mass, and \vec{p} is the electron momentum. The electron velocity is a function of \vec{p} and is given by

$$\vec{v}(\vec{p}) = \vec{\nabla}_p \epsilon = (\vec{p}/m^*)(1 + 2p^2/m^*\epsilon_G)^{-1/2}. \quad (2)$$

In the presence of a magnetic field H , the equation of motion is

$$\dot{\vec{p}} = -e \sum_j \vec{E}_j e^{i\omega_j t} - (e/c) \vec{v} \times \vec{H}, \quad (3)$$

where the applied electric field \vec{E} is expanded in Fourier components and ω_j takes on both positive

and negative values. Equations (2) and (3) are a coupled set of equations from which we may find \vec{p} and \vec{v} to all orders in the applied electric field. Substituting Eq. (2) into (3) we write

$$\dot{\vec{p}} = -e \sum_j \vec{E}_j e^{i\omega_j t} - (1 + 2p^2/m^*\epsilon_G)^{-1/2} \vec{p} \times \vec{\omega}_c, \quad (4)$$

where $\omega_c = eH/m^*c$ is the cyclotron frequency for electrons at the band edge.

Before proceeding we note that all of the important features of our calculation appear if we use a truncated band structure by keeping only the first nonparabolic term in the expansion of Eq. (1), namely

$$\epsilon \cong p^2/2m^* - p^4/4(m^*)^2\epsilon_G. \quad (5)$$

This expansion is valid for $p^2/2m^* \ll \epsilon_G$, which implies that the conduction band is filled only to a Fermi level $\epsilon_F \ll \epsilon_G$. For a conduction-band carrier concentration of $n = 3 \times 10^{16} \text{ cm}^{-3}$, $\epsilon_F/\epsilon_G \sim 0.1$ in InSb, and this assumption starts to break down. However, the details of the following algebraic procedure look considerably simpler with the truncated band structure and we will use it in what follows. At the end of this section the results obtained when the full band structure, Eq. (1), is used will be summarized.

With Eq. (5), Eqs. (2) and (4) become

$$\vec{v}(\vec{p}) = (\vec{p}/m^*)(1 - p^2/m^*\epsilon_G) \quad (6)$$

and

$$\dot{\vec{p}} = -e \sum_j \vec{E}_j e^{i\omega_j t} - (1 - p^2/m^*\epsilon_G) \vec{p} \times \vec{\omega}_c. \quad (7)$$

The next step is to expand p in a series of terms of different order in E_j , $\vec{p} = \vec{p}^{(0)} + \vec{p}^{(1)} + \vec{p}^{(2)} + \vec{p}^{(3)} + \dots$, where $\vec{p}^{(0)}$ is the unperturbed electron momentum (unperturbed means in the absence of applied electric field \vec{E} but in the presence of the magnetic field \vec{H}), $\vec{p}^{(1)}$ is linear, $\vec{p}^{(2)}$ quadratic, and $\vec{p}^{(3)}$ cubic in E .

For convenience, let us now introduce a notation for the circular frame of reference established by the presence of a magnetic field along the \hat{z} direction. The three, independent, nonorthogonal, unit vectors will be $\hat{e}_+ = (\hat{x} - i\hat{y})/\sqrt{2}$, $\hat{e}_- = (\hat{x} + i\hat{y})/\sqrt{2}$, and \hat{z} . Then the vector $\vec{V} = V_x\hat{x} + V_y\hat{y} + V_z\hat{z}$ may be rewritten as $\vec{V} = \vec{V}_+ + \vec{V}_- + \vec{V}_z = V_+\hat{e}_+ + V_-\hat{e}_- + V_z\hat{z}$, where $V_\pm = (V_x \pm iV_y)/\sqrt{2}$. This notation has the nice feature that $\vec{V}_\pm \times \hat{z} = \mp i\vec{V}_\pm$. One must always be careful to distinguish between a vector quantity (e.g., \vec{V}_+) and an amplitude (e.g., V_+). As an illustration we note that

$$\vec{V}_+ - \vec{V}_- = i(\vec{V} \times \hat{z}) = (V_+ - V_-)\hat{y} = \sqrt{2} iV_y\hat{y}. \quad (8)$$

Now starting with Eq. (7), we find $\vec{p}^{(0)}$ by setting $E = 0$. Then, we have

$$\dot{\vec{p}}^{(0)} = -[1 - (p^{(0)})^2/m^*\epsilon_G] \vec{p}^{(0)} \times \vec{\omega}_c. \quad (9)$$

In this semiclassical treatment we shall not quantize the transverse components of momentum into Landau levels. But because of the magnetic field, the unperturbed electrons will move in helices with the axis of the helix in the \hat{z} direction. The \hat{x}, \hat{y} motion will be periodic with an angular frequency given by

$$\omega_c^0 = \omega_c [1 - (p^{(0)})^2 / m^* \epsilon_G] . \quad (10)$$

Thus the model says that the effective cyclotron frequency of each electron differs depending on its *total* unperturbed momentum. This directly reflects the nonparabolicity which results in a different effective mass, and hence a different cyclotron frequency for electrons at different points in the band. Note that ω_c^0 is not time dependent. It depends only on $(p^{(0)})^2$, which is time independent.

Next we solve for $p^{(1)}$. We write $\vec{p}^{(1)} = \vec{p}^{(1)}(\omega_j) \times e^{i\omega_j t}$. Then, from Eq. (7), we have

$$i\omega_j \vec{p}^{(1)}(\omega_j) = -e\vec{E}_j - [\vec{p}^{(1)}(\omega_j) \cdot \vec{\nabla}_p] \\ \times [(1 - p^2/m^* \omega_c) \vec{p} \times \vec{\omega}_c] |_{p=p^{(0)}} .$$

The expression on the right-hand side means that the p derivative of $(1 - p^2/m^* \epsilon_G) \vec{p} \times \vec{\omega}_c$ is to be evaluated at $p = p^{(0)}$. Thus, we have

$$i\omega_j \vec{p}^{(1)}(\omega_j) = -e\vec{E}_j - \vec{p}^{(1)}(\omega_j) \times \vec{\omega}_c^0 \\ + (2/m^* \epsilon_G) (\vec{p}^{(0)} \cdot \vec{p}^{(1)}(\omega_j)) \vec{p}^{(0)} \times \vec{\omega}_c . \quad (11)$$

We will keep only those terms on the right-hand side of Eq. (11) which have no time dependence since we have already taken only one Fourier component of $p^{(1)}$, namely $p^{(1)}(\omega_j) e^{i\omega_j t}$, and dropped the common factor $e^{i\omega_j t}$. Terms from the right-hand side with a time dependence such as $e^{i\omega_c^0 t}$ rightly belong to an analog of Eq. (11) where the Fourier component of $p^{(1)}$ on the left-hand side would be $p^{(1)}(\omega_j + \omega_c^0)$. Such components exist but they are not of interest to us because they contribute only to a higher order in ϵ_F/ϵ_G . The solution of Eq. (11) is

$$p_{\pm}^{(1)}(\omega_j) = ieE_{j\pm} / (\omega_j \mp \omega_c'') , \quad p_z^{(1)}(\omega_j) = ieE_{jz} / \omega_j . \quad (12)$$

ω_c'' is defined by

$$\omega_c'' = \omega_c \{ 1 - [2(p_1^{(0)})^2 + (p_z^{(0)})^2] / m^* \epsilon_G \} . \quad (13)$$

We see that $p^{(1)}(\omega_j)$ has a resonance for $\omega_j = \omega_c''$ (not ω_c). This is the normal cyclotron resonance. Note that for the conditions of YBW's experiment, $\omega_c, \omega_c^0, \omega_c'' \ll \omega_1, \omega_2, \omega_3$ even for the largest magnetic field. Thus certain resonances, such as those in $p^{(1)}(\omega_j)$, are never observed. The method of solution for $p^{(1)}(\omega_j)$ illustrates the basic techniques with which we shall now derive higher-order components of the momentum. For sim-

plicity we shall henceforth write $p^{(1)}(\omega_j) = p(\omega_j)$.

Consider the component $\vec{p}^{(2)}$. This will have frequency components at $\Delta\omega = \omega_1 - \omega_2$ and $2\omega_1$ and also at $\Delta\omega \pm \omega_c^0$ and $2\omega_1 \pm \omega_c^0$, all of which are of the same order in $(p^{(0)})^2$. Lax *et al.*⁹ ignored $\vec{p}^{(2)}$, but they took into account terms which contributed to $\vec{v}(\omega_3)$ in a lower order in $(p^{(0)})^2$. However, it is the contribution of terms containing $\vec{p}^{(2)}$ that become resonant for the relatively low magnetic fields employed by YBW. Taking only the Fourier component with the time dependence $e^{i\Delta\omega t}$ we have from Eq. (7),

$$i\Delta\omega \vec{p}^{(2)}(\Delta\omega) = -\{ [\vec{p}^{(2)}(\Delta\omega) \cdot \vec{\nabla}_p] \\ + [\vec{p}(\omega_1) \cdot \vec{\nabla}_p][\vec{p}(-\omega_2) \cdot \vec{\nabla}_p] \} \\ \times [(1 - p^2/m^* \epsilon_G) \vec{p} \times \vec{\omega}_c] |_{p=p^{(0)}} . \quad (14)$$

Again, taking only time-independent terms on the right-hand side we get

$$i\Delta\omega \vec{p}^{(2)}(\Delta\omega) = -\vec{p}^{(2)}(\Delta\omega) \times \omega_c'' \\ + (2/m^* \epsilon_G) [p_z(\omega_1) p_z^{(0)} \vec{p}(-\omega_2) \times \vec{\omega}_c \\ + p_z(-\omega_2) p_z^{(0)} \vec{p}(\omega_1) \times \vec{\omega}_c] ,$$

which yields the result

$$p_{\pm}^{(2)}(\Delta\omega) = \mp (2\omega_c/m^* \epsilon_G) (\Delta\omega \mp \omega_c'')^{-1} \\ \times [p_z(\omega_1) p_z^{(0)} \vec{p}_{\pm}(-\omega_2) + p_z(-\omega_2) p_z^{(0)} \vec{p}_{\pm}(\omega_1)] . \quad (15)$$

One can understand the result of Eq. (15) by recognizing that the driving term for $\vec{p}^{(2)}(\Delta\omega)$ is $\vec{v} \times \vec{H}$. Due to the nonparabolicity, $p^{(2)}$ has a cubic term in p as shown by Eq. (7). Clearly, the direction of the force is given by the vector $\vec{p} \times \vec{\omega}_c$, which must be normal to \hat{z} and involve a component of p normal to \hat{z} . The three cofactors p in this cubic term must be a $p(\omega_1)$, a $p(-\omega_2)$ and a $p_z^{(0)}$, so that the product goes as $e^{i\Delta\omega t}$. Then, either $\vec{p}(\omega_1)$ or $\vec{p}(-\omega_2)$ must have a perpendicular component and the other must have a \hat{z} component. If both are perpendicular or parallel to \hat{z} then $p^{(2)}(\Delta\omega)$ vanishes since there is no driving force. Resonance occurs when the driving frequency $|\Delta\omega|$ coincides with ω_c'' . These vector relationships are illustrated in Fig. 3(a).

The momentum components with a time dependence $e^{i(\Delta\omega \pm \omega_c^0)t}$ are found from an equation just like Eq. (14).

We find

$$\vec{p}_{\pm}^{(2)}(\Delta\omega - \omega_c^0) = - (4\omega_c/m^* \epsilon_G) (\Delta\omega - \omega_c^0 - \omega_c'')^{-1} \\ \times [\vec{p}_{\pm}^{(0)} \cdot \vec{p}_{\pm}(\omega_1)] \vec{p}_{\pm}(-\omega_2) , \quad (16a)$$

$$\vec{p}_{\pm}^{(2)}(\Delta\omega + \omega_c^0) = (4\omega_c/m^* \epsilon_G) (\Delta\omega + \omega_c^0 + \omega_c'')^{-1} \\ \times [\vec{p}_{\pm}^{(0)} \cdot \vec{p}_{\pm}(\omega_1)] \vec{p}_{\pm}(-\omega_2) , \quad (16b)$$

$$\vec{p}_-^{(2)}(\Delta\omega - \omega_c^0) \propto (\Delta\omega - \omega_c^0 + \omega_c'')^{-1}, \quad (17a)$$

$$\vec{p}_+^{(2)}(\Delta\omega + \omega_c^0) \propto (\Delta\omega + \omega_c^0 - \omega_c'')^{-1}, \quad (17b)$$

and

$$p_x^{(2)}(\Delta\omega - \omega_c^0) = p_x^{(2)}(\Delta\omega + \omega_c^0) = p_x^{(2)}(\Delta\omega) = 0. \quad (18)$$

Since the two expressions given by Eq. (17) are not resonant for the (low) range of magnetic fields we are considering, we need not be concerned with their precise form. In fact, we will not consider them further. A similar argument to that used above can be applied to understand Eq. (16).

Figure 3(b) shows the vector relationships. Here the driving frequency is $|\Delta\omega \pm \omega_c^0|$, and resonance occurs when this is coincident with ω_c'' . Alternatively, when $|\Delta\omega| = |\omega_c^0 + \omega_c''|$ we see a resonance. The resonances at $|\Delta\omega| = |\omega_c'' - \omega_c^0|$ are not observable unless we go to much higher magnetic fields.

Expressions similar to Eqs. (15)–(18) result from considering $2\omega_1$ instead of $\Delta\omega$. However, these become resonant only at much higher magnetic fields and will not be considered.

Due to time-reversal symmetry, there is no SHG or second-order difference mixing (i. e. coherent radiation emitted at $\Delta\omega$) from conduction electrons in InSb. Even though an individual electron may have a momentum component such as $p^{(2)}(\Delta\omega)$, and therefore a velocity component at $\Delta\omega$, this component is proportional to $p^{(0)}$. When the current is found by summing the velocity over all electrons, there is complete cancellation between electrons in time-reversed states. For each electron (momentum $p^{(0)}$), with a given contribution $\delta v(\Delta\omega)$ to the current at $\Delta\omega$, the time-reversed electron (momentum $-p^{(0)}$) contributes $-\delta v(\Delta\omega)$. The lack of radiation at $\Delta\omega$ from conduction electrons may naively be interpreted as implying that no electrons have second-order momentum components $p^{(2)}$. In fact, as we have explicitly shown for this case, each electron may have a component such as $p^{(2)}(\Delta\omega)$, and the next step is to show how this may combine with another $p^{(1)}$ and $p^{(0)}$ to give a nonvanishing macroscopic current at a frequency such as $\omega_3 = 2\omega_1 - \omega_2$.

First observe that one may also find $p^{(3)}(\omega_3)$. It will be proportional to $\omega_c/(\omega_3 \pm \omega_c'')$ and will also be ignored since it is small for the largest fields used by YBW.

We find the third-order current $\vec{v}(\omega_3)$ from Eq. (6). This may be expressed as

$$\vec{v}(\omega_3) \equiv \{[\vec{p}(\omega_1) \cdot \vec{\nabla}_p]^2 [\vec{p}(-\omega_2) \cdot \vec{\nabla}_p]$$

$$\vec{v}(\omega_3) = (1/m^{*2}\epsilon_c) \{ [p(\omega_1)]^2 \vec{p}(-\omega_2) + 2[\vec{p}(\omega_1) \cdot \vec{p}(-\omega_2)] \vec{p}(\omega_1) \} + (1/m^{*2}\epsilon_c) [4(p_x^{(0)})^2/m^* \epsilon_c] \\ \times \left(\omega_c(\Delta\omega - \omega_c'')^{-1} \{ [p_x(\omega_1)]^2 \vec{p}_x(-\omega_2) + p_x(-\omega_2) p_x(\omega_1) \vec{p}_x(\omega_1) + [\vec{p}_-(\omega_1) \cdot \vec{p}_+(\omega_1)] \vec{p}_x(-\omega_2) + [\vec{p}_+(-\omega_2) \cdot \vec{p}_-(\omega_1)] \vec{p}_x(\omega_1) \} \right)$$

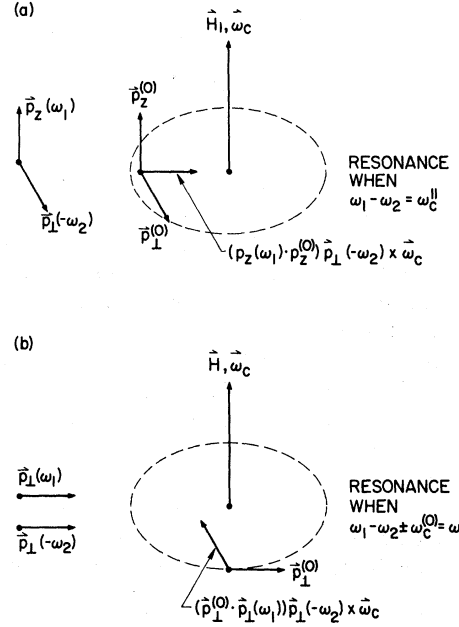


FIG. 3. Relationship between the various momentum components and the force term which drives the electrons in circular orbits in the plane normal to \vec{H} . In (a) the driving force has a time dependence $e^{i(\omega_1 - \omega_2)t}$ whereas in (b) the time dependence is $e^{i(\omega_1 - \omega_2 \pm \omega_c^0)t}$.

$$+ [\vec{p}^{(2)}(\Delta) \cdot \vec{\nabla}_p] [\vec{p}(\omega_1) \cdot \vec{\nabla}_p] \vec{v}(\vec{p})|_{p=p^{(0)}}. \quad (19)$$

Here,

$$\vec{p}^{(2)}(\Delta) = \vec{p}^{(2)}(\Delta\omega) + \vec{p}^{(2)}(\Delta\omega - \omega_c^0) + \vec{p}^{(2)}(\Delta\omega + \omega_c^0).$$

Using Eq. (6), Eq. (19) becomes

$$\vec{v}(\omega_3) = - (1/m^{*2}\epsilon_c) \{ [p(\omega_1)]^2 \vec{p}(-\omega_2) \\ + 2[\vec{p}(\omega_1) \cdot \vec{p}(-\omega_2)] \vec{p}(\omega_1) \\ - (2/m^{*2}\epsilon_c) \{ [\vec{p}^{(2)}(\Delta) \cdot \vec{p}^{(0)}] \vec{p}(\omega_1) \\ + [\vec{p}^{(0)} \cdot \vec{p}(\omega_1)] \vec{p}^{(2)}(\Delta) \\ + [\vec{p}(\omega_1) \cdot \vec{p}^{(2)}(\Delta)] \vec{p}^{(0)} \} \}. \quad (20)$$

In Eq. (20) we must again be careful to keep only the terms with the correct time dependence. For example, each $p^{(2)}(\Delta\omega - \omega_c^0)$ must have a cofactor $p_x^{(0)}$ as well as $p(\omega_1)$ to produce the net correct time dependence. Taking only these terms, substituting Eqs. (15) and (16) into Eq. (20), and setting $p_-(\Delta\omega - \omega_c^0) = p_+(\Delta\omega + \omega_c^0) = 0$, after considerable rearranging we obtain

$$\begin{aligned}
& -\omega_c(\Delta\omega + \omega_c'')^{-1} \{ [p_x(\omega_1)]^2 \tilde{p}_-(-\omega_2) + p_x(-\omega_2) p_x(\omega_1) \tilde{p}_-(\omega_1) + [\tilde{p}_-(\omega_1) \cdot \tilde{p}_+(\omega_1)] \tilde{p}_-(-\omega_2) + [\tilde{p}_-(-\omega_2) \cdot \tilde{p}_+(\omega_1)] \tilde{p}_-(\omega_1) \} \\
& + (1/m^* \epsilon_G) [4(p_1^{(0)})^2/m^* \epsilon_G] [p_x(\omega_1)]^2 [\tilde{p}_-(-\omega_2) \omega_c(\Delta\omega - \omega_c^0 - \omega_c'')^{-1} - \tilde{p}_-(-\omega_2) \omega_c(\Delta\omega + \omega_c^0 + \omega_c'')^{-1}] . \quad (21)
\end{aligned}$$

This important result has the following features. First, there is the nonresonant contribution given by the first term on the right-hand side of Eq. (21). If we use the results of Eq. (21) for $\omega_c = 0$, we simply reproduce the result of Wolff and Pearson.⁷ We call this first term v_{NR} . The two resonant terms each have a factor $(p^{(0)})^2/m^* \epsilon_G$, which, averaged over the Fermi sphere (assuming $kT \ll \epsilon_F$), is proportional to ϵ_F/ϵ_G . In addition, for $H = 0$, $\omega_c = 0$ and these resonant contributions vanish. Thus, if we measure $\chi^{(3)}(H = 0)$ we have a calibrated value with which to compare $\chi^{(3)}(H \neq 0)$ and thereby assess the relative strength of the resonant and nonresonant contributions. Since electrons with different

values of $(p^{(0)})^2$ will have different effective cyclotron frequencies, we see that these electrons will be resonant for different magnetic fields. Thus $\chi^{(3)}$, which results from summing $\tilde{v}(\omega_3)$ over all electrons, will have significant broadening even in the absence of damping.

Equation (21) simplifies considerably when the conditions of YBW's experiment are invoked. In their case, $\vec{E}(\omega_1) \parallel \vec{E}(\omega_2)$ and $\omega_c \ll \omega_1, \omega_2$ and we see from Eq. (12) that $\tilde{p}(\omega_1) \parallel \tilde{p}(\omega_2) \parallel \vec{E}$. We define

$$\omega_c' = \frac{1}{2}(\omega_c^0 + \omega_c'') = \omega_c \left[1 - \left[\frac{3}{2}(p_1^{(0)})^2 + (p_x^{(0)})^2 \right] / m^* \epsilon_G \right]. \quad (22)$$

Then, we have

$$\begin{aligned}
\tilde{v}(\omega_3) = & - (3/m^* \epsilon_G) [p(\omega_1)]^2 \tilde{p}(-\omega_2) + (4\omega_c/m^* \epsilon_G) [(p_x^{(0)})^2/m^* \epsilon_G] [(\Delta\omega)^2 - (\omega_c'')^2]^{-1} \\
& \times \left(\{ 2[p_x(\omega_1)]^2 \tilde{p}_-(-\omega_2) + [p_x(\omega_1)]^2 \tilde{p}_x(-\omega_2) \} (\Delta\omega - \omega_c'') - \{ 2[p_x(\omega_1)]^2 \tilde{p}_+(-\omega_2) + [p_x(\omega_1)]^2 p_x(-\omega_2) \} (\Delta\omega + \omega_c'') \right) \\
& + (4\omega_c/m^* \epsilon_G) [(p_1^{(0)})^2/m^* \epsilon_G] [p_x(\omega_1)]^2 [\tilde{p}_-(-\omega_2) (\Delta\omega - 2\omega_c') - \tilde{p}_+(-\omega_2) (\Delta\omega + 2\omega_c')] [(\Delta\omega)^2 - (2\omega_c')^2]^{-1}. \quad (23)
\end{aligned}$$

For the colinear geometry appropriate to the experiment of YBW, \vec{H} is along \hat{z} , and the propagation vectors \vec{k} of all the light waves are normal to \hat{z} . With $\tilde{p}^{(1)} \parallel \vec{E}$, $\tilde{p}^{(1)}$ is normal to \vec{k} and \vec{H} . The combination $\tilde{p}_-(-\omega_2) - \tilde{p}_+(-\omega_2) = -i(\tilde{p}_1(-\omega_2) \times \hat{z})$ is in the direction of \vec{k} and therefore does not contribute to the radiation. So, in rearranging Eq. (23) we omit terms containing this combination.

In terms of the angle θ between \vec{E} and \vec{H} , we have $|p_x| = |p| \sin\theta$ and $|p_z| = |p| \cos\theta$. Also \hat{e}_E is the unit vector in the \vec{E} direction, $\hat{e}_x = \hat{z}$, and \hat{e}_1 is the unit vector normal to \hat{z} and \vec{k} . Then the result is

$$\begin{aligned}
\tilde{v}(\omega_3) = & - (3/m^* \epsilon_G) [p(\omega_1)]^2 |p(-\omega_2)| \\
& \times \left\{ \hat{e}_E - \frac{16}{3} \omega_c \omega_c'' [(\Delta\omega)^2 - (\omega_c'')^2]^{-1} [(p_x^{(0)})^2/2m^* \epsilon_G] \right. \\
& \times (\sin^2\theta \cos\theta \hat{e}_x + \cos^2\theta \sin\theta \hat{e}_1) \\
& \left. - \frac{16}{3} \omega_c \omega_c' [(\Delta\omega)^2 - (2\omega_c')^2]^{-1} \right. \\
& \left. \times [(p_1^{(0)})^2/2m^* \epsilon_G] \sin^3\theta \hat{e}_1 \right\}. \quad (24)
\end{aligned}$$

The total current at ω_3 is found by summing over electrons.

$$\vec{J}(\omega_3) = - (e/V) \sum_{\text{cond. band}} \tilde{v}(\omega_3), \quad (25)$$

where V is the volume of the crystal. In the approximation of a spherical band given by Eq. (5), Eq. (25) becomes

$$\begin{aligned}
\vec{J}(\omega_3) = & - (e/4\pi^3) \int_0^\infty |p^{(0)}|^2 d|p^{(0)}| f(\epsilon) \\
& \times \int_{\text{solid angle}} d\Omega \tilde{v}(\omega_3), \quad (26)
\end{aligned}$$

where $f(\epsilon)$ is the Fermi-Dirac distribution function.

Most of this discussion has been applied to the truncated-energy-band structure given by Eq. (5). The entire procedure may be repeated starting with Eqs. (1)-(3) with the following result:

$$\begin{aligned}
\tilde{v}(\omega_3) = & - (3/m^* \epsilon_G) [p(\omega_1)]^2 |p(-\omega_2)| \left\{ [A^{-3/2} - 8A^{-5/2} ((p^{(0)})^2/2m^* \epsilon_G) + 16A^{-7/2} ((p^{(0)})^2/2m^* \epsilon_G)^2] \hat{e}_E \right. \\
& - \frac{16}{3} \omega_c \omega_c'' [(\Delta\omega)^2 - (\omega_c'')^2]^{-1} [(p_x^{(0)})^2/2m^* \epsilon_G] A^{-3} [1 - 6A^{-1} (p_1^{(0)})^2/2m^* \epsilon_G]^2 (\sin^2\theta \cos\theta \hat{e}_x + \cos^2\theta \sin\theta \hat{e}_1) \\
& \left. - \frac{16}{3} \omega_c \omega_c' [(\Delta\omega)^2 - (2\omega_c')^2]^{-1} [(p_1^{(0)})^2/2m^* \epsilon_G] A^{-3} [1 - 3A^{-1} (p_1^{(0)})^2/2m^* \epsilon_G]^2 \sin^3\theta \hat{e}_1 \right\}. \quad (27a)
\end{aligned}$$

Here $A = 1 + 2(p^{(0)})^2/m^*\epsilon_G$ and

$$\omega_c'' = \omega_c A^{-1/2} [1 - 2A^{-1}(p_1^{(0)})^2/2m^*\epsilon_G] \quad (27b)$$

and

$$\omega_c' = \omega_c A^{-1/2} [1 - A^{-1}(p_1^{(0)})^2/2m^*\epsilon_G] . \quad (27c)$$

Equations (27) are the full band structure analog of Eqs. (13), (22), and (24). Note that the coefficient of \hat{e}_z in the first term of the right-hand side of Eq. (27) has already been averaged over the angular distribution of unperturbed electron momenta in the

conduction band, but not over the radial distribution. The current may be found by using Eq. (27) instead of Eq. (24) in Eq. (26).

To conclude this section we shall discuss the polarization dependence of the resonant enhancement from the point of view of a simplified quantum model. We picture the conduction band in a magnetic field as quantized into Landau levels spaced by energies of $\sim \hbar\omega_c$. In Fig. 4 we show this conduction band. The expression¹¹ for the nonlinear current density at $\omega_3 = 2\omega_1 - \omega_2$ is proportional to a sum of terms like

$$\vec{v}(\omega_3) \approx \frac{\sum_n \rho_n \langle n | \vec{p} | k \rangle \langle k | \vec{p} \cdot \vec{A}(\omega_1) | j \rangle \langle j | \vec{p} \cdot \vec{A}^\dagger(-\omega_2) | i \rangle \langle i | \vec{p} \cdot \vec{A}(\omega_1) | n \rangle}{[\epsilon_k - \epsilon_n - \hbar(2\omega_1 - \omega_2)] [\epsilon_j - \epsilon_n - \hbar(\omega_1 - \omega_2)] (\epsilon_i - \epsilon_n - \hbar\omega_1)} . \quad (28)$$

Here \vec{p} is the momentum operator, n, i, j , and k are the electronic states and A (A^\dagger) is the photon annihilation (creation) operator of the quantized field. The particular matrix element we have written corresponds to the four-photon process depicted in Fig. 4. There are many other contributing processes but this one illustrates the resonant enhancement for $\hbar(\omega_1 - \omega_2) = \epsilon_j - \epsilon_n$. We label the Landau levels by the quantum number l and consider only intraband transitions. The initial state of the four-step process is labeled n . ρ_n is the occupation number of this state.

It is important to realize that nonparabolicity is required for the nonvanishing of the sum given in Eq. (28), where only intraband transitions are considered.¹² But to the first order, we do not consider the effect of nonparabolicity on the selection rules for electric dipole transitions between Landau levels. These are

$$\vec{p} \perp \vec{H} \Rightarrow \Delta l = \pm 1 \quad \text{and} \quad \vec{p} \parallel \vec{H} \Rightarrow \Delta l = 0 .$$

Noting that $\vec{A}(\omega_1) \parallel \vec{E}(\omega_1)$ we consider the following possibilities: (i) When $\vec{E}(\omega_1) \parallel \vec{E}(\omega_2) \parallel \vec{H}$, we must have $j = i = n$. Thus $\epsilon_j - \epsilon_n = 0$ and there is no enhancement. This is physically reasonable since the electrons are not being driven perpendicular to the magnetic field. (ii) When $\vec{E}(\omega_2) \perp \vec{H}$, and $\vec{E}(\omega_1) \parallel \vec{H}$, then $i = n$, but $j = n \pm 1$, $\epsilon_j - \epsilon_n = \hbar\omega_c$, and we have resonant enhancement when $\omega_1 - \omega_2 = \omega_c$. (iii) If $\vec{E}(\omega_1) \parallel \vec{E}(\omega_2) \perp \vec{H}$, then with $i = n + 1$, and $j = i + 1 = n + 2$ we find $\epsilon_j - \epsilon_n = 2\hbar\omega_c$, and we have resonant enhancement when $\omega_1 - \omega_2 = 2\omega_c$. These rules are consistent with the results of our semiclassical model which shows the proper dependence on the angle between $\vec{E}(\omega_1) \parallel \vec{E}(\omega_2)$ and \vec{H} .

We also note the consistency with the results of spontaneous Raman scattering⁶ where it was found that for laser light propagating parallel to \vec{H} , and therefore $\vec{E}_L \perp \vec{H}$, Stokes-scattered light showed the

following properties:

$$\omega_s = \omega_L - \omega_c \quad \text{with} \quad \vec{E}_s \parallel \vec{H}$$

and

$$\omega_s = \omega_L - 2\omega_c \quad \text{with} \quad \vec{E}_s \perp \vec{H} .$$

III. COMPARISON OF THEORY AND EXPERIMENT

As mentioned above, in the absence of a magnetic field, we have the vanishing of the terms which display resonance. Thus, if we measure the three-wave mixing power in zero magnetic field, we can calibrate our experiment. By this we mean that we keep constant the parameters affecting the laser power, mode structure, focused beam width, etc. and measure the power at ω_3 as a function of magnetic field. YBW noted that the coherence length was constant for their experiment so that all changes in power at ω_3 were due to changes in $\chi^{(3)}$. The current [Eq. (26)] is related to $\chi^{(3)}$ by the relationship $\vec{J}(\omega_3) = i\omega_3 \chi^{(3)} \vec{E}(\omega_1) \vec{E}(\omega_1) \vec{E}(-\omega_2)$. The signal power is proportional to $|\vec{J}(\omega_3)|^2$. YBW wrote $\vec{J}(\omega_3) = \vec{J}_{NR}(\omega_3) + \vec{J}_{RES}(\omega_3)$. They considered J_{NR} to be real and J_{RES} (the resonant contribution) complex. Then, with $|J_{RES}| \ll |J_{NR}|$, they wrote

$$I(\omega_3, H) = \text{const} \times |J(\omega_3, H)|^2$$

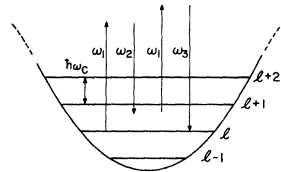


FIG. 4. Plot of ϵ -vs- k_{\perp} (fixed k_{\parallel}) for H along the z direction. With $H \neq 0$ the allowed states condense from the smooth, almost parabolic curve to discrete levels separated by $\sim \hbar\omega_c$. The arrows represent a four-photon process which may show resonant enhancement.

$$\cong \text{const} \times [(J_{NR})^2 + 2(\vec{J}_{NR} \cdot \vec{J}'_{RES})],$$

where J'_{RES} is the real part of J_{RES} . Here $I(\omega_3)$ is the power generated at ω_3 . The normalized power is then

$$\begin{aligned} I(\omega_3, H)/I(\omega_3, 0) &= 1 + 2(\vec{J}_{NR} \cdot \vec{J}'_{RES})/(J_{NR})^2 \\ &= 1 + 2(\chi'_{RES}/\chi_{NR})_{\text{eff}}. \end{aligned} \quad (29)$$

YBW's equation (3) is the result of substituting Eqs. (24) and (26) into Eq. (29). YBW did not actually plot Eq. (29) and compare it in detail to experiment. They recognized the qualitative agreement between theory and experiment, but their statements about the details of the agreement were necessarily vague. Only by numerically calculating $I(\omega_3, H)/I(\omega_3, 0)$ as a function of H , and comparing to experiment can we make more definite statements about the successes and failings of the model. We will do this comparison using both Eqs. (24) and (27). The experimental curves given in Fig. 2 are related to one another through the parameters θ and $\Delta\omega$, the values of which are experimentally known for each of the four curves. Thus, the four curves taken as a group, rather than individually, will be compared to the model.

Unless other values are explicitly specified, we used $\epsilon_G = 0.235$ eV,¹³ $m^* = 0.0137m$,¹⁴ and $T = 15$ °K. Using these values, our first calculated plots showed much too narrow a linewidth with rather sharp peaks, although the resonances occurred at approximately the correct magnetic fields. It became apparent that damping had to be introduced to get a better fit. This is not unexpected in view of the measured mobility of YBW's sample. We carried out a Hall-effect and resistivity measurement on the sample used by YBW. From 4.2 to 77 °K the sample had a mobility $\mu \cong 75\,000$ cm²/V sec from which the relaxation time is calculated to be $\tau = 6 \times 10^{-13}$ sec. In wave numbers one finds $1/\tau \sim 9$ cm⁻¹. This is of the same order as the broadening seen in Fig. 2. Since we don't know what the appropriate relaxation time is for $p^{(2)}$, we leave this as an adjustable parameter and simply replace $\Delta\omega$ by $\Delta\omega - i/\tau$. This is substituted into Eqs. (24) or (27) and the real part of the current is calculated in accordance with Eq. (29).

As for n , the carrier concentration, our Hall-effect measurement gave $n = 5.4 \times 10^{16}$ cm⁻³. Using this value the calculated curves showed amplitude changes at the resonances which were noticeably larger than those of the experimental curves. Thus we treated n as an adjustable parameter. The value of n which provided a good fit thus became one of the criteria by which we could judge the model.

For the truncated band structure [Eq. (24)] we achieved the fit shown in Fig. 5. n and $1/\tau$ were independently varied to achieve this fit. There is

some tradeoff between these two parameters since either larger (smaller) n or larger (smaller) $1/\tau$ tends to broaden (sharpen) the curves and push the structure to larger (smaller) magnetic fields. However, the precise form of the curves depends on n in a different manner from its dependence on $1/\tau$. Figure 6 gives the shape of the curves for a much smaller value of $1/\tau$ in order to show the detrimental effects of almost ignoring relaxation-time broadening. Here n has been correspondingly reduced in order to get a reasonable match of amplitudes. It is clear that the fit in Fig. 6 is inferior to that of Fig. 5. Using the measured value, $n = 5.4 \times 10^{16}$ cm⁻³, the truncated band structure resulted in curves which were grossly in disagreement with the experimental curves, irrespective of what value for τ was used.

The use of the full band structure does not give very different looking results when n and $1/\tau$ are adjusted. A good fit is shown in Fig. 7 and it looks very much like Fig. 5 with some small quantitative

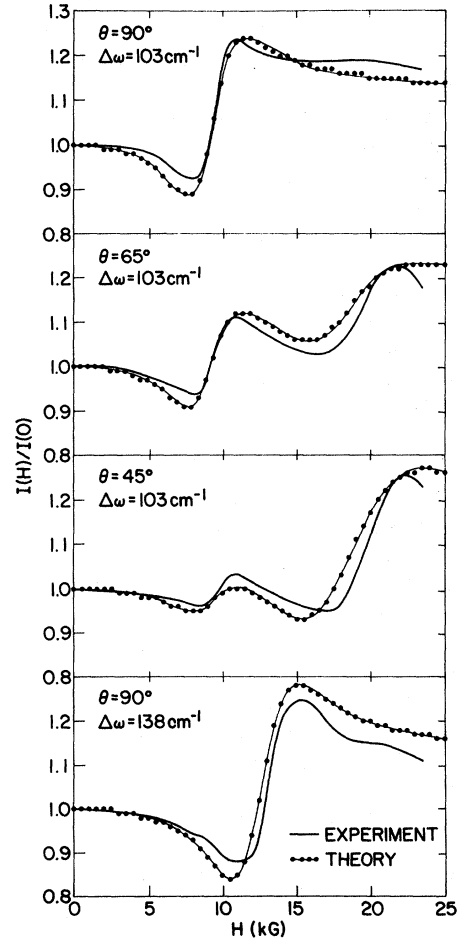


FIG. 5. Comparison of theory and experiment using a truncated band structure [Eq. (24)]. Here $n = 2.19 \times 10^{16}$ cm⁻³ and $1/\tau = 16$ cm⁻¹.

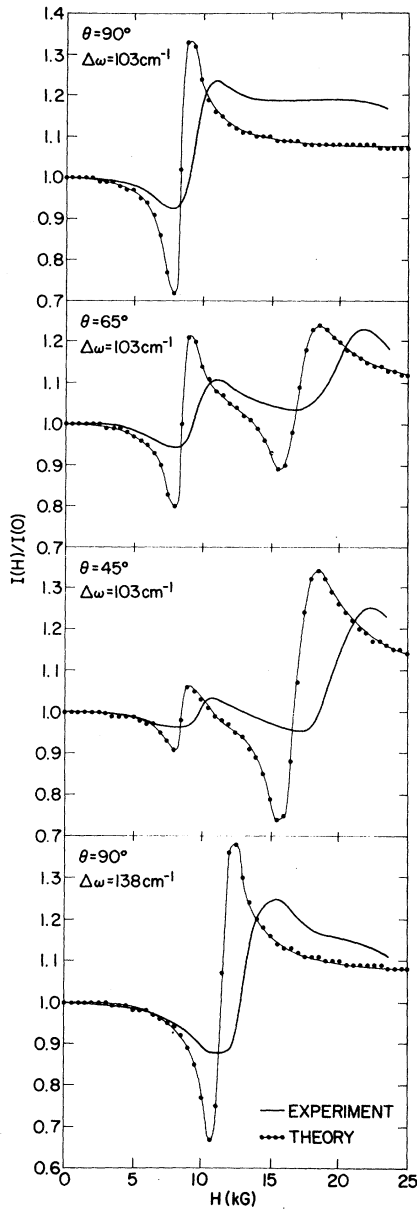


FIG. 6. Comparison using truncated band structure and $n = 9.33 \times 10^{15} \text{ cm}^{-3}$ and $1/\tau = 3 \text{ cm}^{-1}$.

differences. On the other hand for the same values of n and $1/\tau$ as used in obtaining Fig. 5, the full band structure gives a much worse fit.

Although there is not much to choose between Figs. 5 and 7, we note that the n value chosen for the full-band-structure calculation is much closer to that determined from our Hall-effect measurement. Fig. 8 shows the fit obtained using the measured value of n and a slightly larger $1/\tau$. The fit is very reasonable although not as good as that of Fig. 7. Thus by this criterion, the full band struc-

ture gives better results than the truncated band structure. Furthermore, the far too small value of n used to obtain Fig. 6 is another indication that relaxation-time damping is an important consideration. We note that in giving values for n with each calculated curve, we were careful to relate n to the Fermi level in a consistent fashion. n was calculated with the truncated or full band structure accordingly.

The broadening built into the model by letting each electron have a different effective cyclotron frequency is not really essential to a good fit to experiment, provided that we treat n as adjustable. The line shape can be adequately accounted for by relaxation-time broadening alone, by a judicious choice of an "average" effective mass. Instead of Eq. (24), we use the expression obtained from Eq. (24) by replacing ω_c , ω_c' , and ω_c'' by an average cyclotron frequency $(\omega_c)_a = eH/m_a^*c$. Then, if we use $m_a^* = m^* = 0.0137m$, we obtain the result shown in Fig. 9. The calculated curves are displaced too far toward lower magnetic fields. This problem is

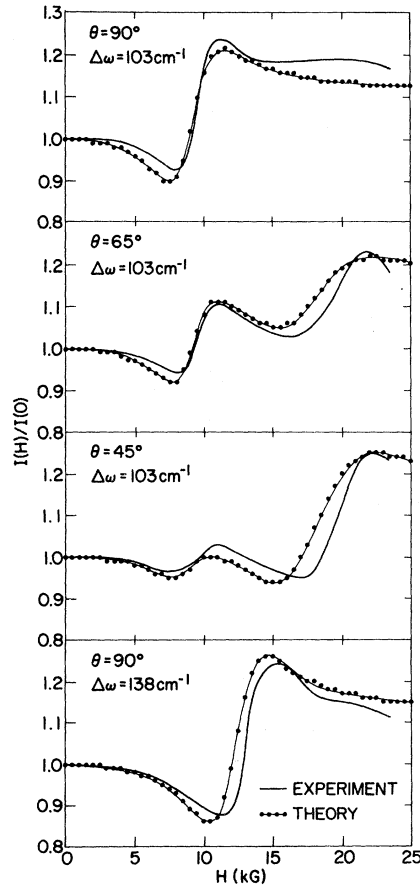


FIG. 7. Comparison using full band structure [Eq. (27)] and $n = 3.46 \times 10^{16} \text{ cm}^{-3}$ and $1/\tau = 17 \text{ cm}^{-1}$.

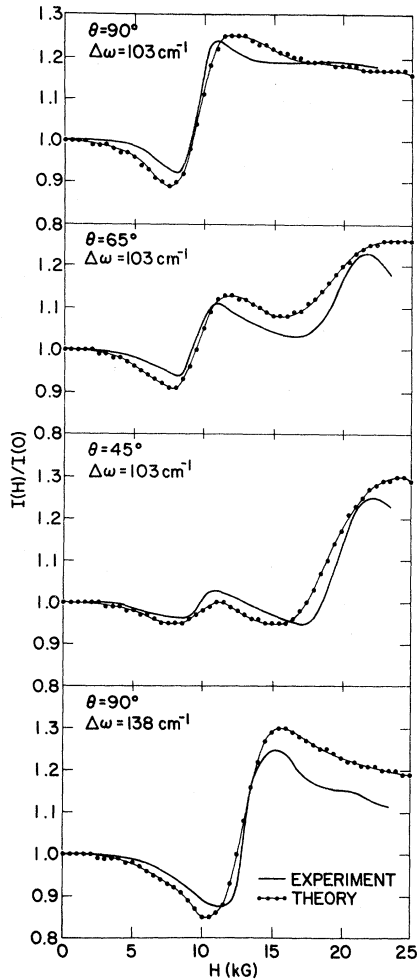


FIG. 8. Comparison using full band structure and $n = 5.4 \times 10^{16} \text{ cm}^{-3}$ and $1/\tau = 19 \text{ cm}^{-1}$.

rectified by the use of $m_a^* = 0.0172m$ which produces the excellent fit shown in Fig. 10. We expect m_a^* to be larger than m^* since electrons other than those at $k = 0$ have an effective mass greater than the value at the band edge. This is just due to the nonparabolicity which results in an ϵ -vs- k curve which is progressively flatter as one moves away from $k = 0$. The value $m_a^* = 0.0172m$ corresponds to $1/m_a^* = (1/m^*)[1 - (p^{(0)})^2/m^*\epsilon_G]$ where $p^{(0)}$ is chosen at approximately the Fermi level. (This Fermi level is the zero magnetic field level for the value of n used in calculating Fig. 9).

The best fits to the four experimental curves are not perfect but they show that the model displays some of the important features. These are the dependence on θ , the dependence on $\Delta\omega$, the amplitudes, and the general shape including both resonances. As we shall see in Sec. IV, this success is remarkable considering the quantum nature of the real problem, especially at the highest H fields.

IV. DISCUSSION

It should be clear that the semiclassical model is useful in understanding YBW's experimental results. The model has the nice features of easy physical interpretation and no need to resort to the quantum dynamical description of electrons in a large dc magnetic field. However, this is just where the model has its most serious limitations. We see this immediately by considering which Landau levels are occupied at $T = 0^\circ \text{K}$ for a magnetic field of $\sim 20 \text{ kG}$. The correct solution of this problem is a good deal more complicated than is required here. Instead, we can think in terms of a fixed Fermi level $\epsilon_F(H) = \epsilon_F(0)$ for a given concentration of conduction electrons. We also can include the effects of spin by adding a k -independent term to the energy, namely $\pm \frac{1}{2}g\mu_B H$. To the first-order approximation, we find that for $n \cong 3 \times 10^{16} \text{ cm}^{-3}$, $\epsilon_F = 190 \text{ cm}^{-1}$. However, $\hbar\omega_c = \hbar eH/m^*c = 6.8H \text{ cm}^{-1}$ (where H is in units of kG), and $\frac{1}{2}g\mu_B H = 1.1H \text{ cm}^{-1}$, where $g = 48$ for InSb. Thus for a field of 20 kG, the spacing of cyclotron levels of the same spin is $\sim 136 \text{ cm}^{-1}$ and the spin

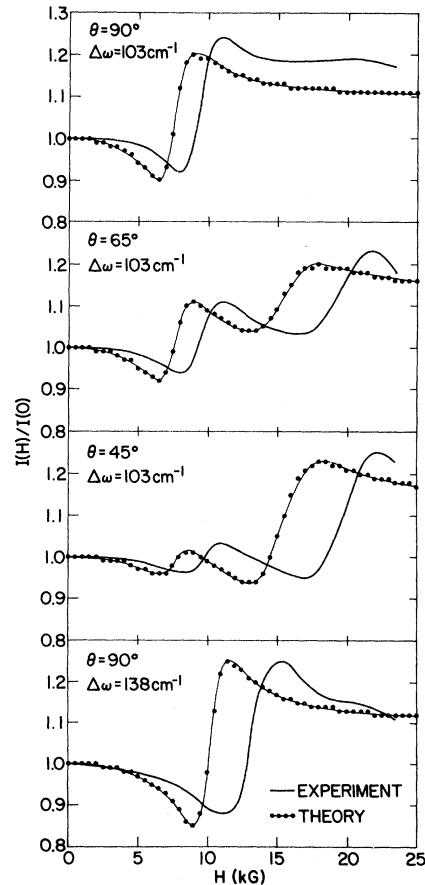


FIG. 9. Comparison using truncated band structure and neglecting broadening in ω_c with $m_a^* = 0.0137m$, $n = 2.19 \times 10^{16} \text{ cm}^{-3}$, and $1/\tau = 17 \text{ cm}^{-1}$.

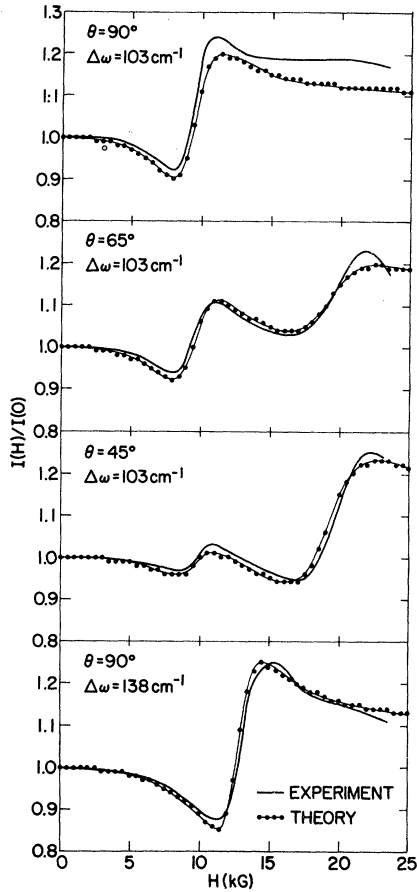


FIG. 10. Comparison using truncated band structure and neglecting broadening in ω_c but with $m_a^* = 0.0172m$, $n = 2.19 \times 10^{16} \text{ cm}^{-3}$, and $1/\tau = 17 \text{ cm}^{-1}$.

splitting is $\sim 44 \text{ cm}^{-1}$. We see that we are approaching the quantum limit for our highest fields and the semiclassical approach is expected to break down. In particular, for the unperturbed electrons, $p_1^{(0)}$ is no longer a good quantum number and it is incorrect to consider the electrons as having a continuous distribution of $p_1^{(0)}$ and a corresponding distribution in ω_c' and ω_c'' . On the other hand, the correct solution shows that ω_c , which really represents the splitting between two levels with $\Delta l = \pm 1$, is a function of $p_x^{(0)}$ and will therefore have a continuous distribution. This partially justifies the semiclassical approach.

At a field of 20 kG, using the above approximation values, only the $(l=0, s=+\frac{1}{2})$, $(l=0, s=-\frac{1}{2})$, and $(l=1, s=+\frac{1}{2})$ levels would be occupied. Clearly, for lower fields more Landau levels are occupied and our approach increases in validity. This seems to be an explanation of why our curves calculated from Eqs. (24) and (27) fit the experiment much better at lower fields than at higher fields. The calculated curves are too broad for the higher resonance ($\Delta\omega \cong \omega_c$). If we restricted the broadening

by replacing $(p_1^{(0)})^2/2m^*\epsilon_G$ in ω_c' and ω_c'' by $(l+\frac{1}{2})\hbar\omega_c/\epsilon_G$ and letting l take on only discrete values, the resonances would certainly sharpen and probably fit better. We did let ω_c take on a fixed value for all electrons (Figs. 9 and 10). The resulting excellent fit, shown in Fig. 10, points up to the fact that the precise distribution of ω_c is not so important, provided that n is suitably adjusted.

The use of an adjustable value for n in the calculations is necessary to get curves which have the correct amplitude. We see that our model attributes a resonant contribution to each electron which is too large relative to the nonresonant contribution. This fault of the model is highly dependent on the choice of band structure as can be seen by the difference between Fig. 5 and 7. Perhaps here also a quantum approach would improve matters. In any case, the full band structure is clearly the best of the models we have considered. Using $n = 5.4 \times 10^{16} \text{ cm}^{-3}$ only the full band structure gives a reasonable fit to experiment, as shown in Fig. 8.

If one wishes to incorporate more of the quantum features, it seems wise to go completely over to a quantum approach. This appears to be necessary in order to include the effects of the electron spin. YBW were limited by the maximum field (23 kG) available from their magnet, and were not able to see the resonance for $\Delta\omega = g\mu_B H$. This would have required a field of $\sim 50 \text{ kG}$ for $\Delta\omega \sim 100 \text{ cm}^{-1}$.⁶ Certainly for this field we would be in the quantum limit and our approach would completely break down. On the other hand, if one chooses a smaller $\Delta\omega$, it might be possible to see the resonant contribution of the spin-flip type of transitions for fields as low as 23 kG. However, we see no way to incorporate the effects of spin into our semiclassical approach. There is no classical analog of the spin comparable to our picture of electrons moving in circular orbits as a classical analog to electrons quantized in Landau levels.

In conclusion, we have discussed a semiclassical model describing the resonant contribution of conduction electrons in InSb to the three wave mixing in a magnetic field. The model is useful in predicting the size of the resonant enhancement and the polarization dependence.

ACKNOWLEDGMENTS

I wish to thank Eli Yablonovitch for his collaboration in the early stages of this work and for many fruitful discussions. Dr. S. S. Jha provided an invaluable assistance in explaining some of the quantum-mechanical aspects of this problem. I am grateful to the IBM Zurich Research Laboratory and its staff for providing computational and other services during my stay at that laboratory. I thank Dr. John Armstrong for a critical reading of the manuscript and for useful comments.

- ¹R. A. Soref and H. W. Moos, *J. Appl. Phys.* **35**, 2152 (1964).
²R. K. Chang, J. Ducuing, and N. Bloembergen, *Phys. Rev. Letters* **15**, 415 (1965).
³F. C. Parsons and R. K. Chang, *Opt. Commun.* **3**, 173 (1971).
⁴J. J. Wynne, *Phys. Rev. Letters* **27**, 17 (1971).
⁵E. Yablonovitch, N. Bloembergen, and J. J. Wynne, *Phys. Rev. B* **3**, 2060 (1971).
⁶R. E. Slusher, C. K. N. Patel, and P. A. Fleury, *Phys. Rev. Letters* **18**, 77 (1967); C. K. N. Patel and R. E. Slusher, *Phys. Rev.* **167**, 413 (1968).
⁷P. A. Wolff and G. A. Pearson, *Phys. Rev. Letters* **17**, 1015 (1966).
⁸C. K. N. Patel, R. E. Slusher, and P. A. Fleury, *Phys. Rev. Letters* **17**, 1011 (1966).
⁹B. Lax, W. Zawadzki, and M. H. Weiler, *Phys. Rev. Letters* **18**, 462 (1967).
¹⁰E. O. Kane, *J. Phys. Chem. Solids* **1**, 249 (1957).
¹¹P. N. Butcher and T. P. McLean, *Proc. Phys. Soc. (London)* **81**, 219 (1963).
¹²P. A. Wolff, *Phys. Rev. Letters* **16**, 225 (1966).
¹³C. R. Pidgeon and R. N. Brown, *Phys. Rev.* **146**, 575 (1966).
¹⁴N. Van Tran and C. K. N. Patel, *Phys. Rev. Letters* **22**, 463 (1969).

PHYSICAL REVIEW B

VOLUME 6, NUMBER 2

15 JULY 1972

Optical Properties of Substitutional Donors in ZnSe

J. L. Merz, H. Kukimoto, K. Nassau, and J. W. Shiever
Bell Telephone Laboratories, Murray Hill, New Jersey 07974

(Received 22 March 1972)

Five substitutional donors have been observed in ZnSe: Al, Ga, In, Cl, and F. By measuring the I_2 lines and the two-electron transitions associated with each, the donor binding energies have been determined. These are found to be close to the effective-mass value and vary from 26.3 meV for Al to 29.3 meV for F. Excited states of the complex formed by the exciton bound to the neutral donor were observed both in the region above the I_2 lines and in the two-electron transitions. The electron effective mass was measured from the Zeeman splitting of the $2p$ states of the donors to be $m = (0.16 \pm 0.01)m_e$. For each donor, a doublet was also observed at lower energy than the I_2 lines; these doublets are believed to be the corresponding I_3 lines. The binding energies of excitons both to the ionized and the neutral donors were found to vary linearly with the donor central-cell correction. Most of these results are closely analogous to the properties of CdS and CdSe.

I. INTRODUCTION

Considerable progress has been made recently toward understanding the nature of donors and acceptors in the II-VI compounds CdS and CdSe by studying the optical properties of large numbers of these crystals which have been systematically doped with the appropriate impurities. Through a detailed study of the Cl donor in CdS, Henry and Nassau¹ unraveled the complicated two-electron transitions and identified excited states of the exciton bound to the neutral donor, the so-called I_2 line. This was extended by Nassau *et al.*,² who determined the chemical identity and binding energies of six substitutional donors in CdS. The same authors have recently studied the optical properties of shallow acceptors in CdS and CdSe,³ and have identified the two-electron transitions of a donor in CdSe.⁴ Comparatively little is known about the substitutional impurities in the Zn compounds, however. In particular, the properties of ZnSe, a wide band gap (~ 2.8 eV), n -type semiconductor which exists in either the cubic or hexagonal form, are little understood.

In this paper, the properties of the substitutional

donors in cubic ZnSe are investigated in detail. The I_2 lines resulting from the radiative recombination of excitons bound to neutral donors have been chemically identified for five different donors, along with the corresponding I_3 lines (excitons bound to the ionized donors). Two-electron transitions are also identified for four of the donors. These transitions also result from the radiative recombination of an exciton bound to a neutral donor, but instead of leaving the donor in its ground $1s$ state (which gives the I_2 line), the donor electron is left in an excited state ($2s$, $2p$, etc.). Two-electron transitions were first identified in GaP,⁵ and shortly thereafter were observed by Reynolds *et al.* in the II-VI compounds CdS,⁶ CdSe,⁷ and ZnO.⁸ In addition to these two-electron transitions in ZnSe, it is also found that a number of two-electron transitions arise from excited states of the three-particle bound exciton complex, that is, the two electrons and one hole that are bound to the ionized donor impurity. Such excited states have also been seen by Henry *et al.*,^{1,4} and by Malm and Haering⁹ using luminescence excitation experiments in CdS. A fifth donor (F) has been identified by the observation of its I_3 lines.